

Electron Waiting Times in a Strongly Interacting Quantum Dot: Interaction Effects and Higher-Order Tunneling Processes

Philipp Stegmann,^{1,*} Björn Sothmann,¹ Jürgen König,¹ and Christian Flindt²

¹*Theoretische Physik, Universität Duisburg-Essen and CENIDE, 47048 Duisburg, Germany*

²*Department of Applied Physics, Aalto University, 00076 Aalto, Finland*

(Dated: August 26, 2021)

Distributions of electron waiting times have been measured in several recent experiments and have been shown to provide complementary information compared to what can be learned from the electric current fluctuations. Existing theories, however, are restricted to either weakly coupled nanostructures or phase-coherent transport in mesoscopic conductors. Here, we consider an interacting quantum dot and develop a real-time diagrammatic theory of waiting time distributions that can treat the interesting regime, in which both interaction effects and higher-order tunneling processes are important. Specifically, we find that our quantum-mechanical theory captures higher-order tunneling processes at low temperatures, which are not included in a classical description, and which dramatically affect the waiting times by allowing fast tunneling processes inside the Coulomb blockade region. Our work paves the way for systematic investigations of temporal fluctuations in interacting quantum systems, for example close to a Kondo resonance or in a Luttinger liquid.

Introduction.— Electronic waiting time distributions are an important concept in the analysis of quantum transport in nano-scale structures [1–36], and recently they have been measured in several experiments [37–42]. Unlike full counting statistics, which typically considers the time-integrated current fluctuations [43–45], waiting time distributions are concerned with the short time-span that passes between the charge transfers in a nanoscale conductor. The waiting time distribution contains a wealth of information about the underlying transport processes. For example, it has been predicted that the waiting time distribution for a quantum point contact should exhibit a cross-over from Wigner-Dyson statistics at full transmission to Poisson statistics close to pinch-off [4, 9], illustrating a profound connection between free fermions and the eigenvalues of random matrices [46].

Experimentally, waiting time distributions have been used to demonstrate accurate control of the emission time statistics of a dynamic single-electron transistor [22, 41] and to characterize the splitting of Cooper pairs in the time domain [26, 36, 42]. Theoretically, electron waiting time distributions have been considered in two opposite regimes. For sequential tunneling in nanostructures, the waiting time distribution can be obtained from a master equation description of the charge transport [1, 3, 35]. On the other hand, for phase-coherent transport of non-interacting electrons, the waiting time distribution can be evaluated using scattering theory [4, 7, 9], tight-binding calculations [12], or Green’s function methods [11, 14]. However, for the interesting intermediate regime, where both interaction effects and higher-order tunneling processes are important, a systematic theory of electronic waiting time distributions has so far been lacking.

In this Letter, we investigate the temporal fluctuations of charge tunneling in a Coulomb-blockade quantum dot and develop a real-time diagrammatic theory of electron waiting time distributions that can treat both strong in-

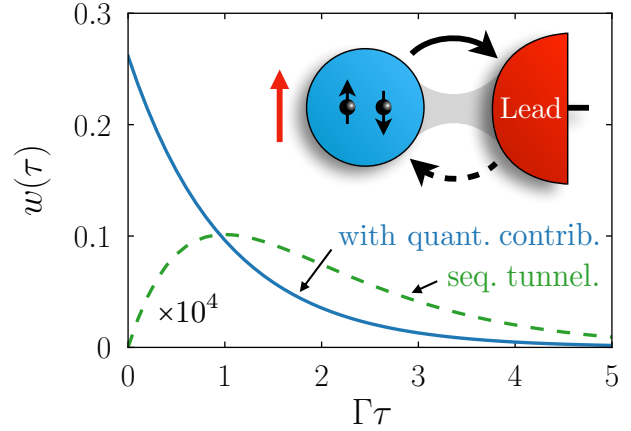


FIG. 1. Electron waiting times for an interacting quantum dot in a magnetic field. Electrons tunnel back and forth (arrows) between the quantum dot and an external reservoir. We consider the waiting time between electrons leaving the quantum dot (full arrow). Waiting time distributions are shown for lowest-order sequential tunneling only (green curve) as well as with higher-order processes included (blue curve). The level position with respect to the chemical potential of the lead is $\varepsilon = -0.2U$, where U is the Coulomb interaction, and the magnetic field causes the Zeeman splitting $\Delta = 1.1U$. The temperature and the coupling are $k_B T = U/30$, $\hbar\Gamma = 10^{-7}U$.

teractions and higher-order tunneling processes [47–49]. Cotunneling processes can be described at the level of mean currents using T -matrix approaches [48–50], which, however, cannot account for non-Markovian effects that influence the charge transport fluctuations beyond average values [51, 52]. Our setup is illustrated in Fig. 1, where we also show waiting time distributions for sequential tunneling only as well as with higher-order tunneling processes included. As we will see, the higher-order tunneling processes are predominantly of quantum nature,

and they tend to get washed out by an increasing electronic temperature for which we recover a classical description based on sequential tunneling. While we here focus on quantum dots, it will become clear that our approach can be applied to a wide range of interacting nanostructures at low temperatures and bias voltages, where quantum effects are important [53–59].

Hamiltonian.— We start by considering a quantum dot coupled to a single electrode before extending the discussion to a transport setup with both a source and a drain electrode. The full Hamiltonian of the setup reads

$$\hat{\mathcal{H}} = \hat{\mathcal{H}}_{\text{qd}} + \hat{\mathcal{H}}_{\text{res}} + \hat{\mathcal{H}}_{\text{tun}}, \quad (1)$$

where the quantum dot, $\hat{\mathcal{H}}_{\text{qd}} = \sum_{\sigma} \varepsilon_{\sigma} \hat{d}_{\sigma}^{\dagger} \hat{d}_{\sigma} + U \hat{d}_{\uparrow}^{\dagger} \hat{d}_{\uparrow} \hat{d}_{\downarrow}^{\dagger} \hat{d}_{\downarrow}$, can be either empty $|0\rangle$, occupied by a single electron $|\sigma\rangle$ with spin $\sigma = \uparrow, \downarrow$, or doubly occupied $|d\rangle$, with U denoting the onsite Coulomb interactions. An applied magnetic field lifts the degeneracy of spin-up, $\varepsilon_{\uparrow} = \varepsilon + \frac{\Delta}{2}$, and spin-down electrons, $\varepsilon_{\downarrow} = \varepsilon - \frac{\Delta}{2}$, where Δ is the Zeeman splitting. The orbital energy ε relative to the chemical potential μ of the reservoir can be tuned by an external gate voltage. The reservoir contains non-interacting electrons and is described by the Hamiltonian $\hat{\mathcal{H}}_{\text{res}} = \sum_{\mathbf{k}\sigma} \varepsilon_{\mathbf{k}\sigma} \hat{a}_{\mathbf{k}\sigma}^{\dagger} \hat{a}_{\mathbf{k}\sigma}$, while electron tunneling between the quantum dot and the reservoir is governed by the Hamiltonian $\hat{\mathcal{H}}_{\text{tun}} = \sum_{\mathbf{k}\sigma} (g \hat{a}_{\mathbf{k}\sigma}^{\dagger} \hat{d}_{\sigma} + g^{*} \hat{d}_{\sigma}^{\dagger} \hat{a}_{\mathbf{k}\sigma})$. The tunnel coupling between the quantum dot and the lead is given by $\Gamma = 2\pi |g|^2 \nu / \hbar$, where ν is the density of states in the lead, which is kept at temperature T .

Master equation.— We describe the quantum dot by its density matrix $\hat{\rho}_N(t)$, which is resolved with respect to the number of transferred particles, so that $P_N(t) = \text{Tr}[\hat{\rho}_N(t)]$ is the probability that $N \geq 0$ electrons have tunneled into the reservoir during the time span $[0, t]$ [44, 60, 61]. The dynamics of the quantum dot is governed by the non-Markovian master equation [51, 52, 62, 63]

$$\frac{d}{dt} \hat{\rho}_N(t) = \sum_{N'} \int_0^t dt' \mathbb{W}_{N-N'}(t-t') \hat{\rho}_{N'}(t') + \hat{\gamma}_N(t), \quad (2)$$

where the kernel \mathbb{W} is obtained by evaluating real-time diagrams on the Keldysh contour up to the desired order in the tunnel coupling Γ [47, 64]. The inhomogeneity $\hat{\gamma}_N(t) = \int_{-\infty}^0 dt' \widetilde{\mathbb{W}}_N(t, t') \hat{\rho}_{\text{stat}}$ describes correlations that build up between the quantum dot and the lead before the counting of particles begins at $t = 0$ [6, 52, 62, 68, 69], and it is expressed in terms of a modified kernel $\widetilde{\mathbb{W}}$, which extends to earlier times. The quantum dot evolves from an arbitrary state in the far past and has reached its stationary state $\hat{\rho}_{\text{stat}}$ well before counting begins.

Solving the non-Markovian master equation is a formidable task. However, we can use an operator-valued generalization of the standard generating function technique in Laplace space by introducing the transformed

density matrix $\hat{\rho}_s(z) = \int_0^{\infty} dt e^{-zt} \sum_N s^N \hat{\rho}_N(t)$ together with similar definitions for the kernel and the inhomogeneity. Using these definitions, the solution of Eq. (2) in Laplace space then becomes [6, 52]

$$\hat{\rho}_s(z) = \frac{1}{z - \mathbb{W}_s(z)} [\hat{\rho}_{\text{stat}} + \hat{\gamma}_s(z)], \quad (3)$$

which is a powerful formal result that in principle yields the full distribution of transferred charge for any observation time. As we now will show, it also leads to a systematic theory of electron waiting times in nano-scale conductors, which can include both interaction effects and higher-order tunneling processes.

Electron waiting times.— The waiting time distribution is the probability density that two consecutive tunneling events are separated by the time τ [1]. It can be expressed as $w(\tau) = \langle \tau \rangle \partial_{\tau}^2 \Pi(\tau)$, where $\langle \tau \rangle = -1/[\partial_{\tau} \Pi(0)]$ is the mean waiting time, and $\Pi(\tau) = P_{N=0}(\tau)$ is the idle-time probability that no transfers have occurred during the time span $[0, \tau]$ [4, 9]. Importantly, the idle-time probability can be obtained from Eq. (3) using that $\Pi(z) = \text{Tr}\{\hat{\rho}_{s=0}(z)\}$. By expanding the kernel around $z = 0$, we can return to the time domain and find [64]

$$w(\tau) = \sum_{m=0}^{\infty} \frac{\langle \tau \rangle}{m!} \partial_z^m \text{Tr} \left\{ \mathcal{J}(z) \mathbb{W}_0^m(z) e^{\mathbb{W}_0(z)\tau} \tilde{\mathcal{J}}(z) \hat{\rho}_{\text{stat}} \right\}_{z=0}, \quad (4)$$

which is a general result that enables a systematic analysis of how tunneling processes of different orders contribute to the distribution of waiting times. Here, we have defined the jump operators $\mathcal{J}(z) = \mathbb{W}_1(z) - \mathbb{W}_0(z)$ and $\tilde{\mathcal{J}}(z) = \mathcal{J}(z) + \int_0^{\infty} dt z e^{-zt} \int_{-\infty}^0 dt' [\widetilde{\mathbb{W}}_1(t, t') - \widetilde{\mathbb{W}}_0(t, t')]$, and we note that memory effects are encoded in non-zero derivatives with respect to z . Thus, only the lowest order term ($m = 0$) remains in the Markovian limit, where we recover the well-known result [1]

$$w_M(\tau) = \langle \tau \rangle \text{Tr} [\mathcal{J} e^{\mathbb{W}_0 \tau} \mathcal{J} \hat{\rho}_{\text{stat}}], \quad (5)$$

since the kernel in that case does not depend on z . Equation (5) is useful to evaluate waiting time distributions in the sequential tunneling regime, where the charge transport can be described by a classical rate equation. By contrast, Eq. (4) allows us to consider lower temperatures, where quantum effects become important.

Tunneling processes.— To evaluate the waiting times between electrons tunneling out of the quantum dot, we expand the kernel order-by-order in the tunneling coupling Γ as $\mathbb{W}_s(z) = \sum_{n=1}^{\infty} \mathbb{W}_s^{(n)}(z)$, with similar expressions for the jump operators and the density matrix. Each term is evaluated using the real-time diagrammatic technique for quantum transport in nano-structures [47–49, 64]. Within this framework, we analytically evaluate the waiting time distribution in Eq. (4) up to second order in the coupling and compare our results with the expression in Eq. (5) using sequential tunneling rates [64].

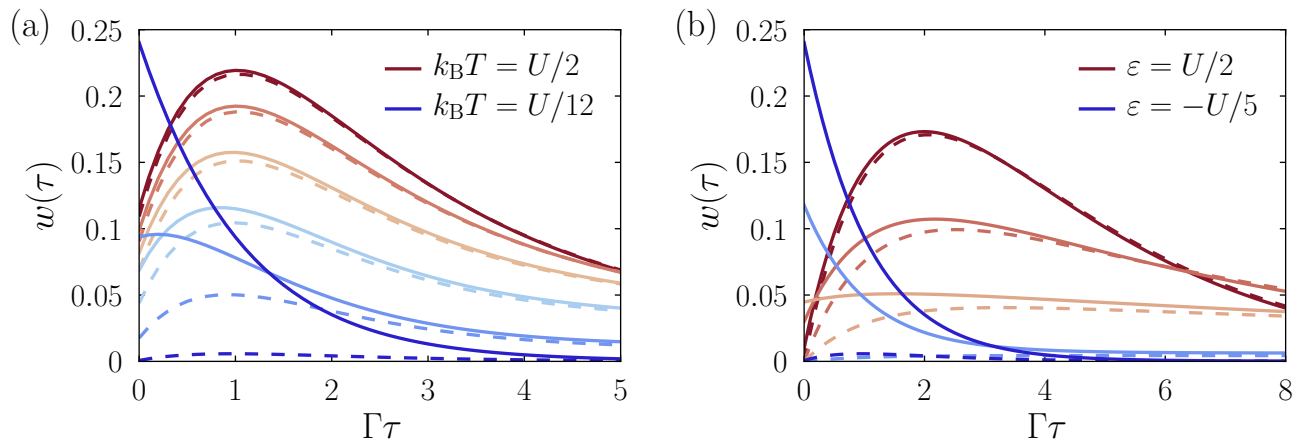


FIG. 2. Distribution of electron waiting times. The quantum mechanical results are based on Eq. (4) evaluated up to second order in the tunnel coupling $\hbar\Gamma = U/60$ (solid lines), while the results for sequential tunneling using Eq. (5) is evaluated up to first order (dashed lines). In panel (a), the temperature is increased in equidistant steps from $k_B T = U/12$ to $k_B T = U/2$, and we use $\varepsilon = -0.2U$ and $\Delta = 1.1U$ for the level position and the Zeeman splitting as in Fig. 1. In panel (b), the level position is $\varepsilon/U = -0.2, 0.1, 0.3, 0.4$, and 0.5 , and the temperature and Zeeman splitting are $k_B T = U/12$ and $\Delta = 1.1U$.

The expansion is controlled by the coupling over the interaction, $\hbar\Gamma/U$. In addition, some sequential tunneling rates get exponentially suppressed at low temperatures and are comparable to second-order processes. Higher-order processes, by contrast, can safely be ignored.

Figure 2 shows distributions of waiting times between electrons tunneling out of the quantum dot as indicated by the full arrow in Fig. 1. Our quantum mechanical calculations are presented with solid lines, while results based on sequential tunneling are indicated with dashed lines. In panel (a), we first focus on waiting time distributions for different electronic temperatures. The state of a single spin-down electron is situated well below the chemical potential of the lead, while the state of a spin-up electron is positioned slightly above the chemical potential. The doubly-occupied state has a larger energy.

At low temperatures, we observe marked differences between the quantum mechanical results that include second-order processes and the classical description based on sequential tunneling only. For the classical description, the quantum dot is likely occupied by a spin-down electron, which energetically is situated below the chemical potential of the lead. It is unlikely that the quantum dot is occupied by a spin-up electron or even doubly-occupied. It only rarely happens that the spin-down electron tunnels out of the quantum dot, which is then quickly refilled by a new spin-down electron, which then tunnels out again much later. Thus, there is a long waiting time between electrons tunneling out of the dot as seen in the corresponding waiting time distribution.

The quantum mechanical results reveal a completely different physical picture with a large peak at short waiting times (solid blue line). The higher-order processes that are now included lead to a renormalized tunnel cou-

pling as well as an increased tunneling rate that makes it possible for the quantum dot to be doubly-occupied [64]. From the doubly-occupied state there are two decay paths with very different dynamics. If the spin-up electron tunnels out first, the quantum dot is left with a spin-down electron, and there will be a long waiting time until this electron leaves the quantum dot. On the other hand, if the spin-down electron first tunnels out, the quantum dot is left in an excited state with the spin-up electron, which then quickly leaves the quantum dot, giving rise to the large peak at short waiting times. Thus, higher-order processes lift the blockade of the tunneling events that occurs when only sequential tunneling is considered.

To corroborate this physical picture, it is instructive to investigate the effects of an increased electronic temperature, where the doubly-occupied state comes into play because of thermal excitations. In this case, the sequential tunneling processes become dominant, and the classical and quantum descriptions in panel (a) coincide as one would expect at high temperatures. A similar behavior is observed in panel (b), where we gradually shift the level upwards, so that the energy of a spin-down electron comes close to the chemical potential, and the blockade is lifted. In this case, the spin-up state and the doubly-occupied state are energetically out of reach, and the classical and quantum mechanical results again agree.

Transport setup.— Having understood the importance of higher-order tunneling processes, we go on to consider a transport setup, where a bias-voltage between two electrodes drives a current through the quantum dot. We consider the waiting time between electrons that tunnel into the drain electrode and evaluate the waiting time distribution up to second order in the equal couplings to the source and the drain electrodes, $\Gamma_S = \Gamma_D$ [64].

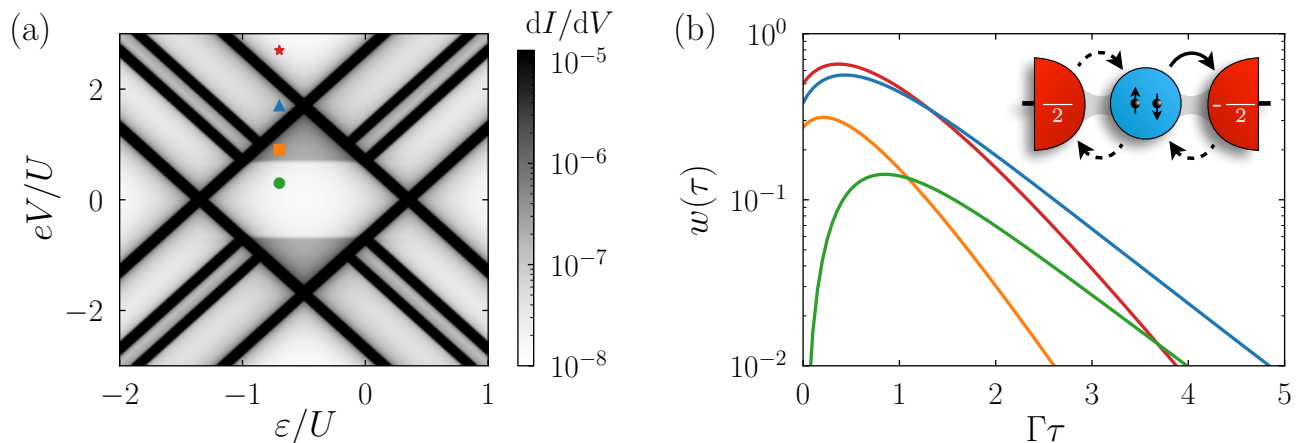


FIG. 3. Waiting time distributions for a transport setup. A bias between two electrodes drives a current through the quantum dot. (a) Differential conductance as a function of the bias-voltage and the gate-voltage. Parameters are $k_B T = U/200$, $\Delta = 0.7U$, and $\Gamma_S = \Gamma_D \equiv \Gamma = 10^{-5}U/\hbar$. (b) Waiting time distributions corresponding to the points in the conductance map.

Figure 3(a) shows a conductance map as a function of the bias-voltage V and the gate voltage, which controls the energy level ε of the quantum dot. In the low-bias regime (green circle), Coulomb blockade suppresses the current in the quantum dot, and elastic cotunneling is the dominant transport mechanism. With an increasing voltage, additional transport processes are activated; first inelastic cotunneling (orange square), then sequential tunneling (blue triangle), and eventually all excitations are inside the bias window such that the Coulomb interactions effectively become irrelevant (red star).

Figure 3(b) shows waiting time distributions corresponding to the four points in the conductance map. At low voltages, the waiting time distribution is suppressed at short times, showing that elastic cotunneling processes rarely occur simultaneously. In this case, the quantum dot mainly makes transitions between being occupied by a spin-down electron and being doubly occupied. As the voltage is increased, the suppression at short times is lifted as inelastic cotunneling gets activated, and the quantum dot can now make transitions from the doubly occupied state to being occupied by a spin-up electron, which quickly leaves via the drain electron before the quantum dot is refilled again. These fast events give rise to the peak at short waiting times, while the long waiting times occur when the quantum dot is occupied by a spin-down electron. As the voltage is further increased, sequential tunneling becomes the main transport mechanism, which can be captured by a classical description as we have checked. Thus, we find that the waiting time distributions can be explained with a classical theory for large bias voltages, while our quantum theory is needed to capture the temporal fluctuations inside the Coulomb blockade region for small voltages and temperatures.

Experimental perspectives.— Finally, we comment on realistic experimental parameters and the perspectives

for measuring the waiting time distributions found here. Taking an interacting strength of about $U \simeq 50 \mu\text{eV}$, the tunneling rate in Fig. 1 would be about $\Gamma \simeq 10 \text{ kHz}$ and the temperature around $T \simeq 30 \text{ mK}$. These parameters are compatible with recent measurements of waiting time distributions [41] and the real-time detection of single-electron tunneling involving virtual processes [70]. Moreover, state-of-the-art setups can detect single electrons on a microsecond timescale [71], corresponding to tunneling rates on the order of $\Gamma \simeq 1 \text{ MHz}$ as in Fig. 3 for $U \simeq 50 \mu\text{eV}$ and $T \simeq 10 \text{ mK}$. In addition, we expect further improvements of charge detectors with bandwidths that are one or two orders of magnitude larger.

Conclusions.— We have investigated the temporal fluctuations of charge tunneling in a quantum dot and developed a real-time diagrammatic theory of electron waiting time distributions that enables a systematic description of interaction effects and higher-order tunneling processes. Our theoretical framework bridges the gap between non-interacting theories of electron waiting times, valid for phase-coherent transport in mesoscopic conductors, and master-equation descriptions, which apply to sequential tunneling in nano-structures with strong interactions. We have found that our quantum mechanical theory captures higher-order tunneling processes at low temperatures, which are not included in a classical description, and which dramatically affect the distribution of waiting times, for example by allowing fast tunneling processes inside the Coulomb blockade region of a quantum dot. Our work paves the way for future investigations of waiting time distributions in systems with strong correlations, for example close to a Kondo resonance [72, 73] or in a Luttinger liquid [74, 75].

Acknowledgements.— We thank A. Braggio for useful discussions. This work was supported by the German Research Foundation (DFG) within the Collabo-

rative Research Centre (SFB) 1242 “Non-Equilibrium Dynamics of Condensed Matter in the Time Domain” (Project No. 278162697) and the Ministry of Innovation NRW via the “Programm zur Förderung der Rückkehr des Hochqualifizierten Forschungsnachwuchses aus dem Ausland”. The work of CF was supported by Academy of Finland through the Finnish Centre of Excellence in Quantum Technology (project nos. 312057 and 312299) and project no. 308515. PS acknowledges support from the German National Academy of Sciences Leopoldina (Grant No. LPDS 2019-10).

* philipp.stegmann@uni-due.de

- [1] T. Brandes, Waiting times and noise in single particle transport, *Ann. Phys.* **17**, 477 (2008).
- [2] S. Welack, S. Mukamel, and Y. Yan, Waiting time distributions of electron transfers through quantum dot Aharonov-Bohm interferometers, *Europhys. Lett.* **85**, 57008 (2009).
- [3] M. Albert, C. Flindt, and M. Büttiker, Distributions of Waiting Times of Dynamic Single-Electron Emitters, *Phys. Rev. Lett.* **107**, 086805 (2011).
- [4] M. Albert, G. Haack, C. Flindt, and M. Büttiker, Electron Waiting Times in Mesoscopic Conductors, *Phys. Rev. Lett.* **108**, 186806 (2012).
- [5] L. Rajabi, C. Pörtl, and M. Governale, Waiting Time Distributions for the Transport through a Quantum-Dot Tunnel Coupled to One Normal and One Superconducting Lead, *Phys. Rev. Lett.* **111**, 067002 (2013).
- [6] K. H. Thomas and C. Flindt, Electron waiting times in non-Markovian quantum transport, *Phys. Rev. B* **87**, 121405 (2013).
- [7] D. Dasenbrook, C. Flindt, and M. Büttiker, Floquet Theory of Electron Waiting Times in Quantum-Coherent Conductors, *Phys. Rev. Lett.* **112**, 146801 (2014).
- [8] M. Albert and P. Devillard, Waiting time distribution for trains of quantized electron pulses, *Phys. Rev. B* **90**, 035431 (2014).
- [9] G. Haack, M. Albert, and C. Flindt, Distributions of electron waiting times in quantum-coherent conductors, *Phys. Rev. B* **90**, 205429 (2014).
- [10] B. Sothmann, Electronic waiting-time distribution of a quantum-dot spin valve, *Phys. Rev. B* **90**, 155315 (2014).
- [11] G.-M. Tang, F. Xu, and J. Wang, Waiting time distribution of quantum electronic transport in the transient regime, *Phys. Rev. B* **89**, 205310 (2014).
- [12] K. H. Thomas and C. Flindt, Waiting time distributions of noninteracting fermions on a tight-binding chain, *Phys. Rev. B* **89**, 245420 (2014).
- [13] D. Dasenbrook, P. P. Hofer, and C. Flindt, Electron waiting times in coherent conductors are correlated, *Phys. Rev. B* **91**, 195420 (2015).
- [14] R. Seoane Souto, R. Avriller, R. C. Monreal, A. Martín-Rodero, and A. Levy Yeyati, Transient dynamics and waiting time distribution of molecular junctions in the polaronic regime, *Phys. Rev. B* **92**, 125435 (2015).
- [15] D. Chevallier, M. Albert, and P. Devillard, Probing Majorana and Andreev bound states with waiting times, *Europhys. Lett.* **116**, 27005 (2016).
- [16] M. Albert, D. Chevallier, and P. Devillard, Waiting times of entangled electrons in normal–superconducting junctions, *Physica E* **76**, 209 (2016).
- [17] T. Brandes and C. Emary, Feedback control of waiting times, *Phys. Rev. E* **93**, 042103 (2016).
- [18] D. Dasenbrook and C. Flindt, Quantum theory of an electron waiting time clock, *Phys. Rev. B* **93**, 245409 (2016).
- [19] P. P. Hofer, D. Dasenbrook, and C. Flindt, Electron waiting times for the mesoscopic capacitor, *Physica E* **82**, 3 (2016).
- [20] S. L. Rudge and D. S. Kosov, Distribution of residence times as a marker to distinguish different pathways for quantum transport, *Phys. Rev. E* **94**, 042134 (2016).
- [21] D. S. Kosov, Waiting time distribution for electron transport in a molecular junction with electron-vibration interaction, *J. Chem. Phys.* **146**, 074102 (2017).
- [22] E. Potanina and C. Flindt, Electron waiting times of a periodically driven single-electron turnstile, *Phys. Rev. B* **96**, 045420 (2017).
- [23] K. Ptaszyński, Waiting time distribution revealing the internal spin dynamics in a double quantum dot, *Phys. Rev. B* **96**, 035409 (2017).
- [24] K. Ptaszyński, Nonrenewal statistics in transport through quantum dots, *Phys. Rev. B* **95**, 045306 (2017).
- [25] K. Ptaszyński, First-passage times in renewal and non-renewal systems, *Phys. Rev. E* **97**, 012127 (2018).
- [26] N. Walldorf, C. Padurariu, A.-P. Jauho, and C. Flindt, Electron Waiting Times of a Cooper Pair Splitter, *Phys. Rev. Lett.* **120**, 087701 (2018).
- [27] G. Tang, F. Xu, S. Mi, and J. Wang, Spin-resolved electron waiting times in a quantum-dot spin valve, *Phys. Rev. B* **97**, 165407 (2018).
- [28] S. Mi, P. Buset, and C. Flindt, Electron waiting times in hybrid junctions with topological superconductors, *Sci. Rep.* **8**, 16828 (2018).
- [29] D. S. Kosov, Waiting time between charging and discharging processes in molecular junctions, *J. Chem. Phys.* **149**, 164105 (2018).
- [30] S. L. Rudge and D. S. Kosov, Distribution of waiting times between electron cotunneling events, *Phys. Rev. B* **98**, 245402 (2018).
- [31] S. L. Rudge and D. S. Kosov, Nonrenewal statistics in quantum transport from the perspective of first-passage and waiting time distributions, *Phys. Rev. B* **99**, 115426 (2019).
- [32] G. Engelhardt and J. Cao, Tuning the Aharonov-Bohm effect with dephasing in nonequilibrium transport, *Phys. Rev. B* **99**, 075436 (2019).
- [33] N. Ho and C. Emary, Counting statistics of dark-state transport through a carbon nanotube quantum dot, *Phys. Rev. B* **100**, 245414 (2019).
- [34] P. Buset, J. Kotilahti, M. Moskalets, and C. Flindt, Time-Domain Spectroscopy of Mesoscopic Conductors Using Voltage Pulses, *Adv. Quantum Technol.* **2**, 1900014 (2019).
- [35] S. L. Rudge and D. S. Kosov, Counting quantum jumps: A summary and comparison of fixed-time and fluctuating-time statistics in electron transport, *J. Chem. Phys.* **151**, 034107 (2019).
- [36] K. Wrześniewski and I. Weymann, Current cross-correlations and waiting time distributions in Andreev transport through Cooper pair splitters based on triple quantum dots, *Phys. Rev. B* **101**, 155409 (2020).
- [37] S. K. Gorman, Y. He, M. G. House, J. G. Keizer,

- D. Keith, L. Fricke, S. J. Hile, M. A. Broome, and M. Y. Simmons, Tunneling Statistics for Analysis of Spin-Readout Fidelity, *Phys. Rev. Applied* **8**, 034019 (2017).
- [38] M. Jenei, E. Potanina, R. Zhao, K. Y. Tan, A. Rossi, T. Tanttu, K. W. Chan, V. Sevriuk, M. Möttönen, and A. Dzurak, Waiting time distributions in a two-level fluctuator coupled to a superconducting charge detector, *Phys. Rev. Research* **1**, 033163 (2019).
- [39] S. Matsuo, K. Kuroyama, S. Yabunaka, S. R. Valentin, A. Ludwig, A. D. Wieck, and S. Tarucha, Full counting statistics of spin-flip and spin-conserving charge transitions in Pauli-spin blockade, *Phys. Rev. Research* **2**, 033120 (2020).
- [40] A. Kurzmann, P. Stegmann, J. Kerski, R. Schott, A. Ludwig, A. D. Wieck, J. König, A. Lorke, and M. Geller, Optical Detection of Single-Electron Tunneling into a Semiconductor Quantum Dot, *Phys. Rev. Lett.* **122**, 247403 (2019).
- [41] F. Brange, A. Schmidt, J. C. Bayer, T. Wagner, C. Flindt, and R. J. Haug, Controlled emission time statistics of a dynamic single-electron transistor, *Sci. Adv.* **7**, eabe0793 (2021).
- [42] A. Ranni, F. Brange, E. T. Mannila, C. Flindt, and V. F. Maisi, Real-time observation of Cooper pair splitting showing strong non-local correlations, [arXiv:2012.10373](https://arxiv.org/abs/2012.10373).
- [43] L. S. Levitov, H. Lee, and G. B. Lesovik, Electron counting statistics and coherent states of electric current, *J. Math. Phys.* **37**, 4845 (1996).
- [44] D. A. Bagrets and Yu. V. Nazarov, Full counting statistics of charge transfer in Coulomb blockade systems, *Phys. Rev. B* **67**, 085316 (2003).
- [45] D. Bagrets, Y. Utsumi, D. Golubev, and G. Schön, Full counting statistics of interacting electrons, *Fortschr. Phys.* **54**, 917 (2006).
- [46] M. L. Metha, *Random Matrices* (Elsevier, Amsterdam, 2004).
- [47] J. König, H. Schoeller, and G. Schön, Zero-bias anomalies and boson-assisted tunneling through quantum dots, *Phys. Rev. Lett.* **76**, 1715 (1996).
- [48] C. Timm, Tunneling through molecules and quantum dots: Master-equation approaches, *Phys. Rev. B* **77**, 195416 (2008).
- [49] S. Koller, M. Grifoni, M. Leijnse, and M. R. Wegewijs, Density-operator approaches to transport through interacting quantum dots: Simplifications in fourth-order perturbation theory, *Phys. Rev. B* **82**, 235307 (2010).
- [50] K. Kaasbjerg and W. Belzig, Full counting statistics and shot noise of cotunneling in quantum dots and single-molecule transistors, *Phys. Rev. B* **91**, 235413 (2015).
- [51] A. Braggio, J. König, and R. Fazio, Full Counting Statistics in Strongly Interacting Systems: Non-Markovian Effects, *Phys. Rev. Lett.* **96**, 026805 (2006).
- [52] C. Flindt, T. Novotný, A. Braggio, M. Sasseti, and A.-P. Jauho, Counting Statistics of Non-Markovian Quantum Stochastic Processes, *Phys. Rev. Lett.* **100**, 150601 (2008).
- [53] M. Ridley, V. N. Singh, E. Gull, and G. Cohen, Numerically exact full counting statistics of the nonequilibrium Anderson impurity model, *Phys. Rev. B* **97**, 115109 (2018).
- [54] M. Ridley, M. Galperin, E. Gull, and G. Cohen, Numerically exact full counting statistics of the energy current in the Kondo regime, *Phys. Rev. B* **100**, 165127 (2019).
- [55] M. Ridley, E. Gull, and G. Cohen, Lead geometry and transport statistics in molecular junctions, *J. Chem. Phys.* **150**, 244107 (2019).
- [56] S. Mundinar, P. Stegmann, J. König, and S. Weiss, Iterative path-integral summations for the tunneling magnetoresistance in interacting quantum-dot spin valves, *Phys. Rev. B* **99**, 195457 (2019).
- [57] M. Kilgour, B. K. Agarwalla, and D. Segal, Path-integral methodology and simulations of quantum thermal transport: Full counting statistics approach, *J. Chem. Phys.* **150**, 084111 (2019).
- [58] C. Schinabeck and M. Thoss, Hierarchical quantum master equation approach to current fluctuations in nonequilibrium charge transport through nanosystems, *Phys. Rev. B* **101**, 075422 (2020).
- [59] A. Erpenbeck, E. Gull, and G. Cohen, Revealing strong correlations in higher order transport statistics: A non-crossing approximation approach, *Phys. Rev. B* **103**, 125431 (2021).
- [60] M. B. Plenio and P. L. Knight, The quantum-jump approach to dissipative dynamics in quantum optics, *Rev. Mod. Phys.* **70**, 101 (1998).
- [61] Yu. Makhlin, G. Schön, and A. Shnirman, Quantum-state engineering with Josephson-junction devices, *Rev. Mod. Phys.* **73**, 357 (2001).
- [62] C. Flindt, T. Novotný, A. Braggio, and A.-P. Jauho, Counting statistics of transport through Coulomb blockade nanostructures: High-order cumulants and non-Markovian effects, *Phys. Rev. B* **82**, 155407 (2010).
- [63] R. Zwanzig, *Nonequilibrium Statistical Mechanics* (Oxford University Press, Oxford, 2001).
- [64] See Supplemental Material for further details. The Supplemental Material includes Refs. [1, 65–67].
- [65] G. D. Mahan, *Many-Particle Physics* (Kluwer, New York, 2000).
- [66] L. S. Levitov and M. Reznikov, Counting statistics of tunneling current, *Phys. Rev. B* **70**, 115305 (2004).
- [67] H. J. Carmichael, S. Singh, R. Vyas, and P. R. Rice, Photoelectron waiting times and atomic state reduction in resonance fluorescence, *Phys. Rev. A* **39**, 1200 (1989).
- [68] D. Marcos, C. Emary, T. Brandes, and R. Aguado, Non-Markovian effects in the quantum noise of interacting nanostructures, *Phys. Rev. B* **83**, 125426 (2011).
- [69] C. Emary and R. Aguado, Quantum versus classical counting in non-Markovian master equations, *Phys. Rev. B* **84**, 085425 (2011).
- [70] S. Gustavsson, M. Studer, R. Leturcq, T. Ihn, K. Ensslin, D. C. Driscoll, and A. C. Gossard, Detecting single-electron tunneling involving virtual processes in real time, *Phys. Rev. B* **78**, 155309 (2008).
- [71] C. Bäuerle, D. C. Glatzli, T. Meunier, F. Portier, P. Roche, P. Roulleau, S. Takada, and X. Waintal, Coherent control of single electrons: a review of current progress, *Rep. Prog. Phys.* **81**, 056503 (2018).
- [72] A. Komnik and A. O. Gogolin, Full Counting Statistics for the Kondo Dot, *Phys. Rev. Lett.* **94**, 216601 (2005).
- [73] T. L. Schmidt, A. O. Gogolin, and A. Komnik, Full counting statistics of spin transfer through a Kondo dot, *Phys. Rev. B* **75**, 235105 (2007).
- [74] A. Komnik and H. Saleur, Full Counting Statistics of Chiral Luttinger Liquids with Impurities, *Phys. Rev. Lett.* **96**, 216406 (2006).
- [75] D. B. Gutman, Y. Gefen, and A. D. Mirlin, Full Counting Statistics of a Luttinger Liquid Conductor, *Phys. Rev. Lett.* **105**, 256802 (2010).

Supplemental Material for Electron Waiting Times in a Strongly Interacting Quantum Dot: Interaction Effects and Higher-Order Tunneling Processes

Philipp Stegmann,^{1,*} Björn Sothmann,¹ Jürgen König,¹ and Christian Flindt²

¹*Theoretische Physik, Universität Duisburg-Essen and CENIDE, 47048 Duisburg, Germany*

²*Department of Applied Physics, Aalto University, 00076 Aalto, Finland*

I. GENERALIZED MASTER EQUATION AND REAL-TIME DIAGRAMMS

We consider a generic transport setup determined by the full Hamiltonian $\hat{\mathcal{H}} = \hat{\mathcal{H}}_{\text{res}} + \hat{\mathcal{H}}_{\text{qs}} + \hat{\mathcal{H}}_{\text{tun}}$. The leads are reservoirs of noninteracting electrons $\hat{\mathcal{H}}_{\text{res}} = \sum_{\mathbf{k}\sigma r} \varepsilon_{\mathbf{k}\sigma r} \hat{a}_{r\mathbf{k}\sigma}^\dagger \hat{a}_{r\mathbf{k}\sigma}$, where $a_{r\mathbf{k}\sigma}^\dagger$ creates an electron with wave vector \mathbf{k} , spin σ , and energy $\varepsilon_{r\mathbf{k}\sigma}$ in the reservoir r . The quantum system of interacting electrons is described by $\hat{\mathcal{H}}_{\text{qs}} = \sum_{\chi} E_{\chi} |\chi\rangle \langle \chi|$ with many-body eigenstates $|\chi\rangle$ at eigenenergies E_{χ} . The quantum system and the reservoir are coupled via a tunneling Hamiltonian $\hat{\mathcal{H}}_{\text{tun}} = \sum_{r\mathbf{k}\sigma m\sigma'} g_{r\mathbf{k}\sigma m\sigma'} \hat{a}_{r\mathbf{k}\sigma}^\dagger \hat{d}_{m\sigma'} + \text{H.c.}$, where $g_{r\mathbf{k}\sigma m\sigma'}$ is the tunnel matrix element and $\hat{d}_{m\sigma'}$ annihilates an electron of the quantum system in orbital m with spin σ' .

We are interested in the time evolution of the reduced density matrix of the quantum system

$$\hat{\rho}(t) = \text{Tr}_{\text{res}}[\hat{\rho}_{\text{full}}(t)] = \sum_{\chi_1, \chi_2} \rho_{\chi_2}^{\chi_1}(t) |\chi_1\rangle \langle \chi_2|, \quad (\text{S1})$$

which is obtained from the density matrix of the full system $\hat{\rho}_{\text{full}}$ by tracing out the reservoir degrees of freedom. We assume that at $t_0 < t$ the full system is in a separable state $\hat{\rho}_{\text{full}}(t_0) = \hat{\rho}(t_0) \otimes \hat{\rho}_{\text{res}}(t_0)$ and the reduced density matrix of the leads $\hat{\rho}_{\text{res}}(t_0)$ is in thermodynamic equilibrium.

The time evolution of the reduced density matrix can formally be written as

$$\rho_{\chi_2}^{\chi_1}(t) = \left\langle (|\chi_2\rangle \langle \chi_1|)(t) \right\rangle = \sum_{\chi'_1, \chi'_2} \rho_{\chi'_2}^{\chi'_1}(t_0) \Pi_{\chi'_2 \chi'_1}^{\chi_1 \chi_2}(t_0, t) \quad (\text{S2})$$

with the *full propagator* in the interaction picture

$$\Pi_{\chi'_2 \chi'_1}^{\chi_1 \chi_2}(t_0, t) = \text{Tr}_{\text{res}} \left[\hat{\rho}_{\text{res}}(t_0) \langle \chi'_2 | \hat{U}_{\text{I}}(t_0, t) (|\chi_2\rangle \langle \chi_1|)(t)_{\text{I}} \hat{U}_{\text{I}}(t, t_0) | \chi'_1 \rangle \right] = \text{Tr}_{\text{res}} \left[\hat{\rho}_{\text{res}}(t_0) \langle \chi'_2 | T_{\text{K}} \hat{U}_{\text{K}} (|\chi_2\rangle \langle \chi_1|)(t)_{\text{I}} | \chi'_1 \rangle \right]. \quad (\text{S3})$$

The full propagator describes the time evolution from the matrix element $\rho_{\chi'_2}^{\chi'_1}(t_0)$ to $\rho_{\chi_2}^{\chi_1}(t)$. Formulated on the *Keldysh contour* K , it gives the time evolution from state χ'_1 at time t_0 to χ_1 at t and then from χ_2 at t backwards to χ'_2 at t_0 . The Keldysh time-ordering operator T_{K} ensures the correct order of the operators along the Keldysh contour. Operators later in the Keldysh time appear further left. The Keldysh time-evolution operator U_{K} can be expanded in powers of the tunneling Hamiltonian

$$T_{\text{K}} \hat{U}_{\text{K}} := T_{\text{K}} \exp \left(-\frac{i}{\hbar} \int_{\text{K}} dt' \hat{\mathcal{H}}_{\text{tun}}(t')_{\text{I}} \right) = \sum_{n=0}^{\infty} \int_{\text{K}} dt_1 \int_{\text{K}} dt_2 \cdots \int_{\text{K}} dt_{2n} \left(-\frac{i}{\hbar} \right)^{2n} T_{\text{K}} \hat{\mathcal{H}}_{\text{tun}}(t_1)_{\text{I}} \hat{\mathcal{H}}_{\text{tun}}(t_2)_{\text{I}} \cdots \hat{\mathcal{H}}_{\text{tun}}(t_{2n})_{\text{I}}, \quad (\text{S4})$$

with $t_1 \geq t_2 \geq \cdots \geq t_{2n}$ in the sense of the Keldysh contour. Since $\hat{\mathcal{H}}_{\text{res}}$ is bilinear in the leads' electron operators, we can apply Wick's theorem [1] to calculate the trace over the reservoir degrees of freedom. Operators $\hat{a}_{\mathbf{k}\sigma r}^\dagger$ and $\hat{a}_{\mathbf{k}\sigma r}$ are *contracted* in time-ordered pairs, which is also the reason why Eq. (S4) includes only even orders of the tunneling Hamiltonian. In contrast, $\hat{\mathcal{H}}_{\text{qs}}$ describes interacting electrons and is, therefore, treated explicitly. We insert identities

* philipp.stegmann@uni-due.de

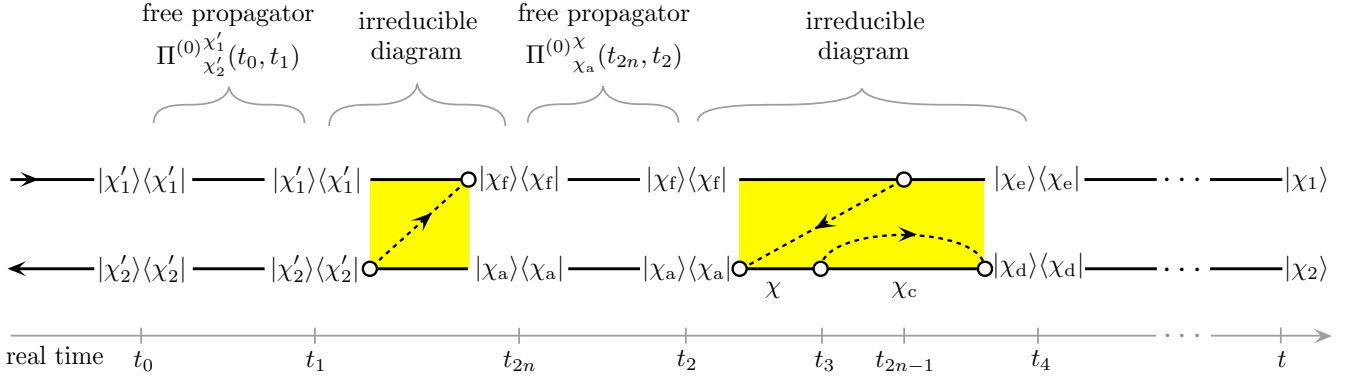


FIG. S1. Real-time dynamics on the Keldysh contour from t_0 to t broken down in free propagators and irreducible diagrams. The illustrated trajectory contributes to $\text{Tr}_{\text{res}} \left[\hat{\rho}_{\text{res}}(t_0) \langle \chi'_2 | \hat{\mathcal{H}}_{\text{tun}}(t_1) \hat{\mathcal{H}}_{\text{tun}}(t_2) \cdots (|\chi_2\rangle \langle \chi_1|)(t) \cdots \hat{\mathcal{H}}_{\text{tun}}(t_{2n}) | \chi'_1 \rangle \right]$.

$\hat{\mathcal{I}} = \sum_{\chi} |\chi\rangle \langle \chi|$ between the tunneling Hamiltonians and perform the remaining calculations in the Schrödinger picture. In conclusion, each time-ordered product of order n

$$\text{Tr}_{\text{res}} \left[\hat{\rho}_{\text{res}}(t_0) \langle \chi'_2 | \hat{\mathcal{H}}_{\text{tun}}(t_1) \hat{\mathcal{H}}_{\text{tun}}(t_2) \cdots (|\chi_2\rangle \langle \chi_1|)(t) \cdots \hat{\mathcal{H}}_{\text{tun}}(t_{2n}) | \chi'_1 \rangle \right]$$

is calculated by summing over all possible *trajectories*, i.e., all combinations of contractions and projectors $|\chi\rangle \langle \chi|$ leading to a nonvanishing value.

Each trajectory can be visualized as illustrated in Fig. S1. Black lines represent free propagating parts of the Keldysh contour, i.e., $\langle \chi | U_0(t', t) | \chi \rangle$ with $\hat{U}_0(t', t) = \exp[-i(\hat{H}_{\text{res}} + \hat{H}_{\text{qs}})(t' - t)/\hbar]$. Contractions are indicated as dashed *tunneling lines*. The open circles on the contour are called *tunneling vertices*. Vertices with a leaving (entering) tunneling line give $\langle \chi' | (-i/\hbar) g_{r\mathbf{k}\sigma m\sigma'} \hat{a}_{r\mathbf{k}\sigma}^\dagger \hat{d}_{m\sigma'} | \chi \rangle$ ($\langle \chi' | (-i/\hbar) g_{r\mathbf{k}\sigma m\sigma'}^* \hat{d}_{m\sigma'}^\dagger \hat{a}_{r\mathbf{k}\sigma} | \chi \rangle$), where χ are the entering and χ' the leaving states. Thus, the emission (absorption) of an electron by the quantum system is indicated by tunneling lines which leave (enter) the vertices.

The time evolution from t_0 and t is separated in *free propagators*

$$\Pi_{\chi_2}^{(0)\chi_1}(t', t) = \langle \chi_2 | U_0(t', t) | \chi_2 \rangle \langle \chi_1 | U_0(t, t') | \chi_1 \rangle = e^{-\frac{i}{\hbar}(E_{\chi_1} - E_{\chi_2})(t-t')} \quad (\text{S5})$$

and *irreducible diagrams* which describe tunneling events between the leads and the quantum system. Irreducible means here that one can not draw a vertical line through these diagrams without cutting a tunneling line.

From the form of the trajectories depicted in Fig. S1, it is immediately clear that we can reformulate the full propagator recursively in the sense of a Dyson equation

$$\Pi_{\chi_2'}^{\chi_1'}(t_0, t) = \Pi_{\chi_2}^{(0)\chi_1}(t_0, t) \delta_{\chi_1', \chi_1} \delta_{\chi_2', \chi_2} + \sum_{\chi_1'', \chi_2''} \int_{t_0}^t dt_2 \int_{t_0}^{t_2} dt_1 \Pi_{\chi_2''}^{\chi_1''}(t_0, t_1) \mathbb{W}_{\chi_2''}^{\chi_1'' \chi_1'}(t_1, t_2) \Pi_{\chi_2}^{(0)\chi_1}(t_2, t). \quad (\text{S6})$$

The integral kernel $\mathbb{W}_{\chi_2'}^{\chi_1'}(t', t)$ is the sum of all possible irreducible diagrams connecting the matrix element $\rho_{\chi_2'}^{\chi_1'}(t')$ with $\rho_{\chi_2}^{\chi_1}(t)$. Hence, the leftmost vertex of each irreducible diagram is at t' and the rightmost vertex is at t .

Inserting Eq. (S6) into Eq. (S2) and differentiating with respect to t yields the *generalized master equation*

$$\frac{d}{dt} \rho_{\chi_2}^{\chi_1}(t) = -\frac{i}{\hbar} (E_{\chi_1} - E_{\chi_2}) \rho_{\chi_2}^{\chi_1}(t) + \sum_{\chi_1', \chi_2'} \int_{t_0}^t dt' \rho_{\chi_2'}^{\chi_1'}(t') \mathbb{W}_{\chi_2}^{\chi_1' \chi_1}(t', t). \quad (\text{S7})$$

The first term on the right-hand side describes the time evolution in the absence of tunneling events. It arises from the free propagator in Eq. (S6). The second term determines the dissipative coupling to the leads. This term forces the quantum system to approach a stationary state. The kernel in Eq. (S7) is written down as function of both t' and t . However, since the system is not explicit time dependent, the kernel depends only on the time difference $t - t'$ and we can write $\mathbb{W}_{\chi_2}^{\chi_1' \chi_1}(t', t) = \mathbb{W}_{\chi_2}^{\chi_1' \chi_1}(t - t')$.

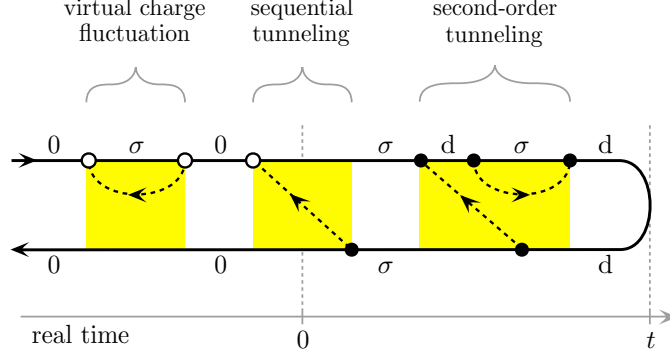


FIG. S2. Real-time dynamics on the Keldysh contour for the Hamiltonian studied in the main text. Counted tunneling vertices after $t = 0$ are shown as filled black circles, while earlier ones are indicated by open circles.

At last, we introduce a detector which does not change the dynamics of the system but counts the number of electrons N that have been transferred through the quantum system in time interval $[0, t]$. We replace the master equation for $\rho_{\chi_2}^{\chi_1}(t)$ by an N -resolved version for $\rho_{N\chi_2}^{\chi_1}(t)$

$$\frac{d}{dt}\rho_{N\chi_2}^{\chi_1}(t) = -\frac{i}{\hbar}(E_{\chi_1} - E_{\chi_2})\rho_{N\chi_2}^{\chi_1}(t) + \sum_{N',\chi'_1,\chi'_2} \int_{t_0}^t dt' \rho_{N'\chi'_2}^{\chi'_1}(t') \widetilde{\mathbb{W}}_{N-N',\chi'_2\chi_2}^{\chi_1\chi_1}(t', t). \quad (\text{S8})$$

The integral kernel $\widetilde{\mathbb{W}}_{N-N',\chi'_2\chi_2}^{\chi_1\chi_1}(t', t)$ includes only those irreducible diagrams that change the detector counter by $N - N'$. The unresolved density matrix and kernel are recovered by summing over N , i.e., $\rho_{\chi_2}^{\chi_1}(t) = \sum_N \rho_{N\chi_2}^{\chi_1}(t)$ and $\mathbb{W}_{\chi'_2\chi_2}^{\chi_1\chi_1}(t', t) = \sum_N \widetilde{\mathbb{W}}_{N-N',\chi'_2\chi_2}^{\chi_1\chi_1}(t', t)$. Time translation invariance is broken at $t' = 0$ due to the switching on of the detector. Therefore, the time dependence of the kernel simplifies to $\widetilde{\mathbb{W}}_{N-N',\chi'_2\chi_2}^{\chi_1\chi_1}(t', t) = \mathbb{W}_{N-N',\chi'_2\chi_2}^{\chi_1\chi_1}(t - t')$ only for $t' \geq 0$. Moreover, $\rho_{N\chi_2}^{\chi_1}(t') = \delta_{N',0} \rho_{\chi_2}^{\chi_1}(t')$ for $t' < 0$. Thus, Eq. (S8) takes the form

$$\frac{d}{dt}\rho_{N\chi_2}^{\chi_1}(t) = -\frac{i}{\hbar}(E_{\chi_1} - E_{\chi_2})\rho_{N\chi_2}^{\chi_1}(t) + \sum_{N',\chi'_1,\chi'_2} \int_0^t dt' \rho_{N'\chi'_2}^{\chi'_1}(t') \mathbb{W}_{N-N',\chi'_2\chi_2}^{\chi_1\chi_1}(t - t') + \sum_{\chi'_1,\chi'_2} \int_{t_0}^0 dt' \rho_{\chi'_2}^{\chi'_1}(t') \widetilde{\mathbb{W}}_{N\chi'_2\chi_2}^{\chi_1\chi_1}(t', t). \quad (\text{S9})$$

The last term is called *inhomogeneity* $\gamma_{N\chi_2}^{\chi_1}(t)$. The kernel $\widetilde{\mathbb{W}}_{N\chi'_2\chi_2}^{\chi_1\chi_1}(t', t)$ is nonvanishing for $t - t'$ being smaller than the memory time of the kernel. If we assume that the system has reached its stationary state earlier, we can set $t_0 \rightarrow -\infty$ and $\rho_{\chi'_2}^{\chi'_1}(t') \rightarrow \rho_{\text{stat}}^{\chi'_1}$. In conclusion, we have recovered Eq. (2) of the main text. There, we concentrated on systems where the density matrix is diagonal and the first term in Eq. (S9) vanishes.

II. DIAGRAMMATIC RULES AND COUNTING FIELDS

In this section, we present rules how to calculate the kernel elements $\mathbb{W}_s^{(n)\chi_1\chi_1}_{\chi'_2\chi_2}(z)$ for the Hamiltonian studied in the main text. The superscript (n) indicates the order in the tunnel-coupling strength $\Gamma_r = 2\pi|g_r|^2\nu_r/\hbar$, where ν_r is the density of states in lead r . The Fermi function of lead r is $f_r^+(\omega) = 1/[e^{(\omega-\mu_r)/k_B T} + 1]$ and $f_r^-(\omega) = 1 - f_r^+(\omega)$. Since counting begins at $t = 0$, only tunneling vertices later in real time, indicated by filled black circles in Fig. S2, contribute to the detector counter. We follow the counting procedure introduced in Ref. 2 and apply the replacement $g_r \rightarrow g_r e^{iX_r/2}$ to filled tunneling vertices on the upper and $g_r \rightarrow g_r e^{-iX_r/2}$ to the ones on the lower Keldysh contour. Afterwards, we change from counting fields to counting factors via the replacement $iX_r \rightarrow \ln s_r$. The resulting counting procedure is summarized in the 4th rule. More details of the counting procedure are given at the beginning of Section III. The rules are:

1. Draw all topologically different irreducible diagrams with n tunneling lines connecting tunneling vertices on either the same or opposite contours. Assign the states χ'_1 , χ_1 , χ'_2 , and χ_2 to the four corners of the diagram and the respective states to the ends of each free propagating part. Furthermore, each free propagating part gets its corresponding energy E_χ as well as each tunneling line its energy ω .

2. For each time interval on the real axis confined by two neighboring vertices (independent if they are on the same or opposite contours), write down a resolvent $1/(\Delta E + iz)$, where ΔE is the energy of the left-going free propagating parts and tunneling lines minus the energy of the right-going ones.
3. Add a factor $\frac{\hbar}{2\pi} f_r^-(\omega)$ for each tunneling line running forward and $\frac{\hbar}{2\pi} f_r^+(\omega)$ for each tunneling line running backwards in the Keldysh time.
4. For each pair of vertices connected by a tunneling line, multiply with

$$s_r^{m/2} \Gamma_r \langle \chi'_4 | \hat{d}_\uparrow | \chi_4 \rangle \langle \chi'_3 | \hat{d}_\uparrow^\dagger | \chi_3 \rangle + s_r^{m/2} \Gamma_r \langle \chi'_4 | \hat{d}_\downarrow | \chi_4 \rangle \langle \chi'_3 | \hat{d}_\downarrow^\dagger | \chi_3 \rangle,$$

where χ_3 and χ_4 (χ'_3 and χ'_4) are the states that enter (leave) the vertex with respect to the Keldysh time. Here, m is the number of filled vertices with beginning tunneling line on the upper or ending tunneling line on the lower contour minus the number of filled vertices with ending tunneling line on the lower or beginning tunneling line on the upper contour.

5. Assign the factor $-\frac{i}{\hbar}(-1)^{b+c}$ where b is the number of vertices on the lower contour and c the number of crossings of tunneling lines.
6. Integrate over all energies ω and sum over the leads r .
7. Sum up the contributions of all diagrams.

III. DIAGRAMMATIC KERNEL

We present the kernel elements obtained from the diagrammatic rules and used to produce Fig. 1, 2, 3(b), and S3. We sum over r and r' in the expression given below. Afterwards, we set $\Gamma_S = 0$, $s_D^{-1} = 1$, and $s_D = s$ in case of Fig. 1, 2, and S3. For the waiting time distribution in Fig. 3(b), we set $s_D^{-1} = s_S^{-1} = s_S = 1$ and $s_D = s$.

The nonvanishing kernel elements in first order in the tunnel-coupling strength read

$$\mathbb{W}_{s_S s_D}^{(1) 0\sigma}(z=0) = \sum_{r=S,D} \frac{1}{s_r} \Gamma_r f_r^+(\varepsilon_\sigma), \quad (\text{S10})$$

$$\mathbb{W}_{s_S s_D}^{(1) \sigma 0}(z=0) = \sum_{r=S,D} s_r \Gamma_r f_r^-(\varepsilon_\sigma), \quad (\text{S11})$$

$$\mathbb{W}_{s_S s_D}^{(1) \sigma d}(z=0) = \sum_{r=S,D} \frac{1}{s_r} \Gamma_r f_r^+(\varepsilon_{\bar{\sigma}} + U), \quad (\text{S12})$$

$$\mathbb{W}_{s_S s_D}^{(1) d\sigma}(z=0) = \sum_{r=S,D} s_r \Gamma_r f_r^-(\varepsilon_{\bar{\sigma}} + U), \quad (\text{S13})$$

$$\mathbb{W}_{s_S s_D}^{(1) \chi\chi}(z=0) = - \sum_{\chi' \neq \chi} \mathbb{W}_{11}^{(1) \chi\chi'}(z=0), \quad (\text{S14})$$

with $\varepsilon_\uparrow = \varepsilon + \frac{\Delta}{2}$ and $\varepsilon_\downarrow = \varepsilon - \frac{\Delta}{2}$. The elements given in Eqs. (S10) - (S13) account for sequential tunneling processes from state χ' to state χ where one electron is exchanged between the leads and the dot. The kernel elements given in Eq. (S14) are determined by virtual charge fluctuations. They ensure the conservation of probability.

The kernel elements which are relevant in the elastic and inelastic cotunneling regime are

$$\mathbb{W}_{s_S s_D}^{(2) \downarrow 0}(z=0) = \sum_{r'r} s_{r'} \Gamma_{\text{ren}}^{\text{sq } r'r}, \quad (\text{S15})$$

$$\mathbb{W}_{s_S s_D}^{(2) \downarrow \uparrow}(z=0) = \sum_{r'r} \frac{s_{r'}}{s_r} \left(\Gamma_{\downarrow \uparrow}^{\text{cot } r'r} + \Gamma_{\text{ren} \downarrow \uparrow}^{\text{cot } r'r} \right), \quad (\text{S16})$$

$$\mathbb{W}_{s_S s_D}^{(2) \downarrow \downarrow}(z=0) = \sum_{r'r} \left(\frac{s_{r'}}{s_r} - 1 \right) \left(\Gamma_{\downarrow \downarrow}^{\text{cot } r'r} + \Gamma_{\text{ren} \downarrow \downarrow}^{\text{cot } r'r} \right) - \sum_{\chi \neq \downarrow} \mathbb{W}_{11}^{(2) \downarrow \chi}(z=0), \quad (\text{S17})$$

$$\mathbb{W}_{s_S s_D}^{(2) \downarrow d}(z=0) = \sum_{r'r} \frac{1}{s_{r'}} \Gamma_{\text{ren} \downarrow d}^{\text{sq } r'r}. \quad (\text{S18})$$

The individual terms involved take the form

$$\Gamma_{\downarrow\downarrow}^{\text{cot } r'r} = \partial_x \gamma(\mu_{r'}, \mu_r, U, 0), \quad (\text{S19})$$

$$\Gamma_{\downarrow\uparrow}^{\text{cot } r'r} = \partial_x \gamma(\mu_{r'}, \mu_r - \Delta, U - \Delta, 0) + \frac{2}{U} \gamma(\mu_{r'}, \mu_r - \Delta, U - \Delta, 0), \quad (\text{S20})$$

$$\Gamma_{\text{ren } \downarrow 0}^{\text{sq } r'r} = -\hbar \Gamma_{r'} \Gamma_r \partial \phi_{r'}(\varepsilon_{\downarrow}) [f_r^+(\varepsilon_{\uparrow}) + f_r^+(\varepsilon_{\downarrow})], \quad (\text{S21})$$

$$\Gamma_{\text{ren } \downarrow\uparrow}^{\text{cot } r'r} = \hbar \Gamma_{r'} \Gamma_r \partial \phi_{r'}(\varepsilon_{\downarrow}) f_r^+(\varepsilon_{\uparrow}) - \hbar \Gamma_{r'} \Gamma_r \partial \phi_{r'}(\varepsilon_{\uparrow} + U) f_r^-(\varepsilon_{\downarrow} + U), \quad (\text{S22})$$

$$\Gamma_{\text{ren } \downarrow\downarrow}^{\text{cot } r'r} = \hbar \Gamma_{r'} \Gamma_r \partial \phi_{r'}(\varepsilon_{\downarrow}) f_r^+(\varepsilon_{\downarrow}) - \hbar \Gamma_{r'} \Gamma_r \partial \phi_{r'}(\varepsilon_{\uparrow} + U) f_r^-(\varepsilon_{\uparrow} + U), \quad (\text{S23})$$

$$\Gamma_{\text{ren } \downarrow\downarrow}^{\text{sq } r'r} = \hbar \Gamma_{r'} \Gamma_r \partial \phi_{r'}(\varepsilon_{\uparrow} + U) [f_r^-(\varepsilon_{\uparrow} + U) + f_r^-(\varepsilon_{\downarrow} + U)], \quad (\text{S24})$$

with $\phi_r(x) = \frac{1}{2} \text{Re} \Psi(\frac{1}{2} + i \frac{x - \mu_r}{2\pi k_{\text{BT}}})$, where $\Psi(x)$ is the digamma function. The elastic and inelastic cotunneling rates $\Gamma_{\downarrow\downarrow}^{\text{cot } r'r}$ and $\Gamma_{\downarrow\uparrow}^{\text{cot } r'r}$ are determined by

$$\gamma(\mu_{r'}, \mu_r, U, x) = \hbar \Gamma_{r'} \Gamma_r f_r^{\text{B}}(\mu_{r'}) [\phi_{r'}(\varepsilon_{\downarrow} + x) - \phi_{r'}(\varepsilon_{\uparrow} + U - x) - \phi_r(\varepsilon_{\downarrow} + x) + \phi_r(\varepsilon_{\uparrow} + U - x)], \quad (\text{S25})$$

with the Bose function $f_r^{\text{B}}(x) = 1/[e^{(x - \mu_r)/k_{\text{BT}}} - 1]$. The remaining terms in Eqs. (S21) - (S24) are second-order corrections due to a renormalized tunnel-coupling strength.

IV. INHOMOGENEITY

The kernel $\widetilde{\mathbb{W}}_s(t, t')$ is build up by probabilities that certain numbers of tunneling vertices occur in the time span $[t', 0]$ and $[0, t]$. The calculation simplifies in leading order in the tunnel-coupling strength. Then, one vertex occurs at $t' < 0$ (not counted) and a second one at $t > 0$ (counted). The kernel $\widetilde{\mathbb{W}}_s^{(1)}(t, t') = \widetilde{\mathbb{W}}_s^{(1)}(t - t')$ depends only on the time difference between those two vertices. The inhomogeneity takes the form

$$\hat{\gamma}_s^{(1)}(t) = \left[\int_{-\infty}^t dt' \widetilde{\mathbb{W}}_s^{(1)}(t - t') - \int_0^t dt' \widetilde{\mathbb{W}}_s^{(1)}(t - t') \right] \hat{\rho}_{\text{stat}}^{(0)}. \quad (\text{S26})$$

Here, we have assumed that $\hat{\rho}_N(t \leq 0) = \delta_{N,0} \hat{\rho}_{\text{stat}}$ and, moreover, extended the kernel $\widetilde{\mathbb{W}}_s^{(1)}(t - t')$ to the domain $0 < t' < t$. The Laplace transform is

$$\hat{\gamma}_s^{(1)}(z) = \frac{1}{z} [\widetilde{\mathbb{W}}_s^{(1)}(0) - \widetilde{\mathbb{W}}_s^{(1)}(z)] \hat{\rho}_{\text{stat}}^{(0)}. \quad (\text{S27})$$

We note that Eq. (S27) holds in arbitrary order if counting fields are not included ($s = 1$)

$$\hat{\gamma}_1(z) = \frac{1}{z} [\mathbb{W}_1(0) - \mathbb{W}_1(z)] \hat{\rho}_{\text{stat}} = -\frac{1}{z} \mathbb{W}_1(z) \hat{\rho}_{\text{stat}}. \quad (\text{S28})$$

V. WAITING TIME DISTRIBUTION

In this section, we derive the non-Markovian form of the waiting time distribution in detail. We start with Eq. (3) of the main text

$$\hat{\rho}_s(z) = \frac{1}{z - \mathbb{W}_s(z)} [\hat{\rho}_{\text{stat}} + \hat{\gamma}_s(z)]. \quad (\text{S29})$$

The prefactor is written in the form of a Neumann series $[1 - \mathbb{W}_s(z)]^{-1} = \sum_{n=0}^{\infty} \mathbb{W}_s^n(z)/z^{n+1}$ and $\mathbb{W}_s^n(z)$ as well as $\hat{\gamma}_s(z)$ are expressed by their Taylor series. We obtain

$$\hat{\rho}_s(z) = \sum_{m,n,k=0}^{\infty} \frac{z^{m+k-n-1}}{m! k!} \left\{ \partial_z^m [\mathbb{W}_s^n(z)] \partial_z^k [\hat{\rho}_{\text{stat}} + \hat{\gamma}_s(z)] \right\}_{z=0}, \quad (\text{S30})$$

where $\partial_z^k \hat{\rho}_{\text{stat}} = \delta_{k,0} \hat{\rho}_{\text{stat}}$. The inverse Laplace transform yields $1/z^{n+1} \rightarrow t^n/n!$ for the negative powers and $z^n \rightarrow \partial_t^n \delta(t)$ for the positive powers in z . We assume finite t and, therefore, neglect terms including a Dirac delta function $\delta(t)$ or its derivatives. Thus, the solution of the master equation reads

$$\hat{\rho}_s(t) = \sum_{m,k=0}^{\infty} \frac{1}{m!k!} \left\{ \partial_z^m \left[\mathbb{W}_s^{m+k}(z) e^{\mathbb{W}_s(z)t} \right] \partial_z^k [\hat{\rho}_{\text{stat}} + \hat{\gamma}_s(z)] \right\}_{z=0}, \quad (\text{S31})$$

which can be simplified by means of the Leibniz rule to

$$\hat{\rho}_s(t) = \sum_{m=0}^{\infty} \frac{1}{m!} \partial_z^m \left\{ \mathbb{W}_s^m(z) e^{\mathbb{W}_s(z)t} [\hat{\rho}_{\text{stat}} + \hat{\gamma}_s(z)] \right\}_{z=0}. \quad (\text{S32})$$

The waiting time distribution $w(\tau) = \langle \tau \rangle \partial_\tau^2 \Pi(\tau)$ can be derived from the mean waiting time $\langle \tau \rangle = -1/[\partial_\tau \Pi(0)]$ and the idle-time probability $\Pi(\tau) = \text{Tr}[\hat{\rho}_{s=0}(\tau)]$. We take into account that $\text{Tr}[\mathbb{W}_1(z)\bullet] = 0$ and $\hat{\gamma}_1(z) = -\mathbb{W}_1(z)\hat{\rho}_{\text{stat}}/z$, see Section IV. The waiting time distribution reads

$$w(\tau) = \sum_{m=0}^{\infty} \frac{\langle \tau \rangle}{m!} \partial_z^m \text{Tr} \left\{ \mathcal{J}(z) \mathbb{W}_0^m(z) e^{\mathbb{W}_0(z)\tau} [\mathcal{J}(z)\hat{\rho}_{\text{stat}} + z\hat{\gamma}_1(z) - \mathbb{W}_0(z)\hat{\gamma}_0(z)] \right\}_{z=0}, \quad (\text{S33})$$

with the jump operator $\mathcal{J}(z) := \mathbb{W}_1(z) - \mathbb{W}_0(z)$. Finally, we use the relation $(m+1)\partial_z^m [f(z)]_{z=0} = \partial_z^{m+1} [f(z)z]_{z=0}$ and

$$\tilde{\mathcal{J}}(z)\hat{\rho}_{\text{stat}} := \mathcal{J}(z) + \int_0^\infty dt z e^{-zt} \int_{-\infty}^0 dt' [\tilde{\mathbb{W}}_1(t, t') - \tilde{\mathbb{W}}_0(t, t')] \hat{\rho}_{\text{stat}} = \mathcal{J}(z) + z[\hat{\gamma}_1(z) - \hat{\gamma}_0(z)] \quad (\text{S34})$$

to obtain Eq. (4) of the main text

$$w(\tau) = \sum_{m=0}^{\infty} \frac{\langle \tau \rangle}{m!} \partial_z^m \text{Tr} \left\{ \mathcal{J}(z) \mathbb{W}_0^m(z) e^{\mathbb{W}_0(z)\tau} \tilde{\mathcal{J}}(z)\hat{\rho}_{\text{stat}} \right\}_{z=0}. \quad (\text{S35})$$

VI. PERTURBATIVE EXPANSIONS

In this section, we expand the waiting time distribution in the tunnel-coupling strength Γ

$$w(\tau) = \langle \tau \rangle \sum_{n=0}^{\infty} \partial_\tau^2 \Pi^{(n)}(\tau) = \langle \tau \rangle \sum_{n=0}^{\infty} \frac{\Gamma^n}{n!} \partial_\Gamma^n [\partial_\tau^2 \Pi(\tau)]_{\Gamma=0}, \quad (\text{S36})$$

with the superscript (n) indicating the order of the tunnel-coupling strength. The product $\Gamma\tau$ is treated as Γ -independent variable in the following. In practice, the infinite sum is truncated at a certain order n_{max} . To preserve the normalization of the waiting time distribution, the mean waiting time is truncated accordingly. Its expansion is directly obtainable from the expansion of $\partial_\tau^2 \Pi(\tau)$ and is one order lower in the coupling strength

$$\langle \tau \rangle_{n_{\text{max}}-1} = \left(\int_0^\infty d\tau \sum_{n=0}^{n_{\text{max}}} \partial_\tau^2 \Pi^{(n)}(\tau) \right)^{-1} = - \left(\sum_{n=0}^{n_{\text{max}}-1} \partial_\tau \Pi^{(n)}(0) \right)^{-1}. \quad (\text{S37})$$

We set $n_{\text{max}} = 2$ to obtain the waiting time distribution in the lowest nonvanishing order. We recover from Eq. (S35) the well-known Markovian form [3, 4]

$$w_1^{\text{M}}(\tau) = \langle \tau \rangle_1 \sum_{n=0}^{n_{\text{max}}=2} \partial_\tau^2 \Pi^{(n)}(\tau) = \langle \tau \rangle_1 \frac{\Gamma^2}{2!} \partial_\Gamma^2 [\partial_\tau^2 \Pi(\tau)]_{\Gamma=0} = \frac{\text{Tr} \left[\mathcal{J}^{(1)} e^{\mathbb{W}_0^{(1)}\tau} \mathcal{J}^{(1)} \hat{\rho}_{\text{stat}}^{(0)} \right]}{\text{Tr} \left[\mathcal{J}^{(1)} \hat{\rho}_{\text{stat}}^{(0)} \right]}. \quad (\text{S38})$$

Here, only first-order processes are involved (sequential tunneling). The Laplace variable z is not written down explicitly. The exponential function $e^{\mathbb{W}_0^{(1)}\tau}$ includes only powers of $\Gamma\tau$ and is, therefore, considered to be independent

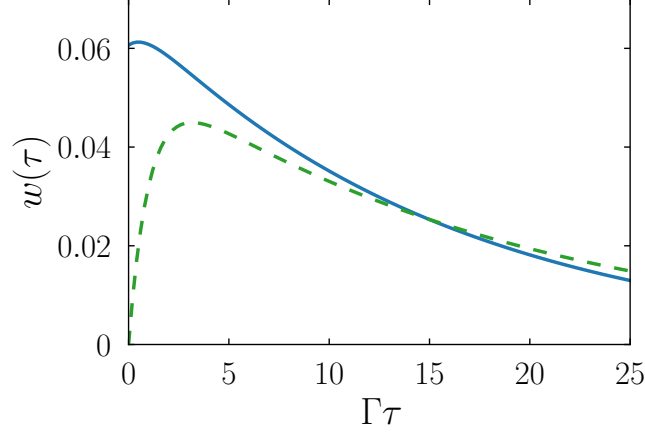


FIG. S3. Distribution of electron waiting times for the setup depicted in Fig. 1 of the main text. The approximation of lowest-order sequential tunneling given in Eq. (S38) (dashed green line) is compared with the full expression given in Eq. (S40) evaluated up to second order in the tunnel-coupling Γ (solid blue line). The level position is $\varepsilon = 0.3U$ and no magnetic field is applied. The temperature and the coupling are $k_B T = U/12$ and $\hbar\Gamma = U/60$.

of Γ . If we include the next-to-leading order ($n_{\max} = 3$), second-order Markovian as well as non-Markovian processes are taken into account. The waiting time distribution reads

$$\begin{aligned} \frac{w_2(\tau)}{\langle \tau \rangle_2} &= \text{Tr}[\mathcal{J}^{(1)} e^{\mathbb{W}_0^{(1)} \tau} \mathcal{J}^{(1)} \hat{\rho}_{\text{stat}}^{(0)}] + \frac{\Gamma^3}{3!} \partial_\Gamma^3 \text{Tr}[(\mathcal{J}^{(1)} + \mathcal{J}^{(2)}) e^{(\mathbb{W}_0^{(1)} + \mathbb{W}_0^{(2)}) \tau} (\mathcal{J}^{(1)} + \mathcal{J}^{(2)}) (\hat{\rho}_{\text{stat}}^{(0)} + \hat{\rho}_{\text{stat}}^{(1)})]_{\Gamma=0} \\ &+ \frac{\Gamma^3}{3!} \partial_\Gamma^3 \partial_z \text{Tr}[\mathcal{J}^{(1)} \mathbb{W}_0^{(1)} e^{\mathbb{W}_0^{(1)} \tau} \tilde{\mathcal{J}}^{(1)} \hat{\rho}_{\text{stat}}^{(0)}]_{\Gamma=0}. \end{aligned} \quad (\text{S39})$$

The first two terms are Markovian and the third term is a non-Markovian correction indicated by the z -derivative. We introduce the auxiliary jump operator $\mathbb{J}^{(2)} = \mathcal{L}_1^{(2)} - \mathcal{L}_0^{(2)}$ with $\mathcal{L}_s^{(2)} = \mathbb{W}_s^{(2)} + (\partial_z \mathbb{W}_s^{(1)}) \mathbb{W}_s^{(1)}$ and obtain the form

$$\begin{aligned} \frac{w_2(\tau)}{\langle \tau \rangle_2} &= \text{Tr}[\mathcal{J}^{(1)} e^{\mathbb{W}_0^{(1)} \tau} \mathcal{J}^{(1)} (\hat{\rho}_{\text{stat}}^{(0)} + \hat{\rho}_{\text{stat}}^{(1)})] + \text{Tr}[\mathbb{J}^{(2)} e^{\mathbb{W}_0^{(1)} \tau} \mathcal{J}^{(1)} \hat{\rho}_{\text{stat}}^{(0)}] + \text{Tr}[\mathcal{J}^{(1)} e^{\mathbb{W}_0^{(1)} \tau} \mathbb{J}^{(2)} \hat{\rho}_{\text{stat}}^{(0)}] \\ &+ \Gamma \text{Tr}[\mathcal{J}^{(1)} \partial_\Gamma [e^{(\mathbb{W}_0^{(1)} + \mathcal{L}_0^{(2)}) \tau}]_{\Gamma=0} \mathcal{J}^{(1)} \hat{\rho}_{\text{stat}}^{(0)}] + \text{Tr}[\mathcal{J}^{(1)} e^{\mathbb{W}_0^{(1)} \tau} \mathbb{W}_0^{(1)} \partial_z \tilde{\mathcal{J}}^{(1)} \hat{\rho}_{\text{stat}}^{(0)}], \end{aligned} \quad (\text{S40})$$

with

$$\frac{1}{\langle \tau \rangle_2} = \text{Tr}[\mathcal{J}^{(1)} (\hat{\rho}_{\text{stat}}^{(0)} + \hat{\rho}_{\text{stat}}^{(1)}) + \mathbb{J}^{(2)} \hat{\rho}_{\text{stat}}^{(0)}] - \text{Tr}[\mathcal{J}^{(1)} \partial_z \tilde{\mathcal{J}}^{(1)} \hat{\rho}_{\text{stat}}^{(0)}]. \quad (\text{S41})$$

The derivative $\partial_\Gamma [e^{(\mathbb{W}_0^{(1)} + \mathcal{L}_0^{(2)}) \tau}]_{\Gamma=0}$ includes only powers of $\Gamma\tau$. In the long-time limit, one may replace it by $e^{(\mathbb{W}_0^{(1)} + \mathcal{L}_0^{(2)}) \tau}$ in order to approximate the slope of the distribution more accurately. The stationary density matrix in leading and next-to-leading order is determined by $(\mathbb{W}_1^{(1)} + \mathbb{W}_1^{(2)}) \hat{\rho}_{\text{stat}} = 0$ with $\text{Tr}[\hat{\rho}_{\text{stat}}] = 1$. Then, $\hat{\rho}_{\text{stat}}^{(0)} = [\hat{\rho}_{\text{stat}}]_{\Gamma=0}$ and $\hat{\rho}_{\text{stat}}^{(1)} = \partial_\Gamma [\hat{\rho}_{\text{stat}}]_{\Gamma=0}$. Non-Markovian terms include the operators $\partial_z \mathbb{W}_s^{(1)}$ or $\partial_z \tilde{\mathbb{W}}_s^{(1)}$. They are neglected under Markov approximation.

VII. MEMORY AND RENORMALIZATION EFFECTS

Our diagrammatic approach yields analytic expressions for the waiting time distribution giving us additional insight into the underlying tunneling dynamics. We obtain for the full waiting time distribution (S40) in Fig. S3 (solid blue line) at $\tau = 0$

$$\frac{w_2(0)}{\langle \tau \rangle_2} = \sum_{\sigma\sigma'} \rho_{\text{stat}\sigma'}^{(0)} \Gamma_{\sigma'0}^{\text{sq}} [\Gamma_{0\sigma}^{\text{sq}} (\partial_z \Gamma_{\sigma 0}^{\text{sq}}) + (\partial_z \Gamma_{0\sigma}^{\text{sq}}) \Gamma_{\sigma 0}^{\text{sq}}] - \sum_{\sigma} \rho_{\text{stat}0}^{(0)} (\partial_z \Gamma_{00}^{\text{vir}}) \Gamma_{0\sigma}^{\text{sq}} \Gamma_{\sigma 0}^{\text{sq}}, \quad (\text{S42})$$

with $\Gamma_{\chi'\chi}^{\text{sq}} = \mathbb{W}_{11}^{(1)\chi'\chi}$ and $\Gamma_{\chi\chi}^{\text{vir}} = \mathbb{W}_{11}^{(1)\chi\chi}$. Derivatives ∂_z indicate the non-Markovian nature of the process. The first (second) term accounts for memory generated after (before) counting starts, i.e., the second (third) term in Eq. (S9). Noteworthy, non-Markovian correction due to virtual charge fluctuations ($\partial_z \Gamma_{00}^{\text{vir}}$) enter via the second term.

The lifting of the short-time suppression in Fig. 1 of the main text is due to second-order Markovian corrections. We obtain

$$\frac{w_2(0)}{\langle \tau \rangle_2} = \rho_{\text{statd}}^{(1)} \Gamma_{d\uparrow}^{\text{sq}} \Gamma_{\uparrow 0}^{\text{sq}}, \quad (\text{S43})$$

at $\tau = 0$ with the density-matrix element $\rho_{\text{statd}}^{(1)} = \Gamma_{\text{ren } \downarrow d}^{\text{sq}} / (2\Gamma)$. The term $\Gamma_{\text{ren } \downarrow d}^{\text{sq}}$ is a correction due to a renormalized tunnel-coupling strength, see Section III. The distribution at $\tau = 0$ becomes most pronounced for $\Delta \approx U$ when the excitation energies $E_d - E_{\uparrow}$ and $E_{\uparrow} - E_0$ align. The suppression is lifted if $|\downarrow\rangle$ is the ground state of the dot (i.e., $-\frac{\Delta}{2} - U < \varepsilon < \frac{\Delta}{2}$). Then, an additional electron enters frequently due to a second-order Markovian tunneling event. Next, a spin- \downarrow electron tunnels out (i.e., $\frac{\Delta}{2} - U < \varepsilon$) followed by a spin- \uparrow electron (i.e., $-\frac{\Delta}{2} < \varepsilon$). In summary, the lifting can be observed for $\max(\frac{\Delta}{2} - U, -\frac{\Delta}{2}) < \varepsilon < \frac{\Delta}{2}$ and, therefore, a nonvanishing Zeeman splitting is required. The criterion is, especially, not fulfilled in Fig. S3.

- [1] G. D. Mahan, *Many-Particle Physics* (Kluwer, New York, 2000).
- [2] L. S. Levitov and M. Reznikov, Counting statistics of tunneling current, *Phys. Rev. B* **70**, 115305 (2004).
- [3] H. J. Carmichael, S. Singh, R. Vyas, and P. R. Rice, Photoelectron waiting times and atomic state reduction in resonance fluorescence, *Phys. Rev. A* **39**, 1200 (1989).
- [4] T. Brandes, Waiting times and noise in single particle transport, *Ann. Phys.* **17**, 477 (2008).